How the Reduced Graphene Oxide Prepared at Different pH Values Affect the Optical Transmittance and the Electrical Properties of Polystrene Latex Films?

Onder Yargi,[1*] **Ali Gelir**,[2] **Utkan Sahinturk**,[3] **Tanju Ozer**,[1] **Murat Caliskan**,[1] **Baki Aksakal**[1]
[1]*Department of Physics Yildiz Technical University, Esenler, 34210, Istanbul, Turkey*

[2]*Department of Physics Istanbul Technical University, Maslak, 34469, Istanbul, Turkey*

[3]*Department of Mechanical and Metal Technology, Vocational School of Technical Sciences, Istanbul University, TR-34320, Istanbul, Turkey*

Optical transmittance and electrical properties of polystyrene (PS)/reduced graphene oxide (rGO) composites were studied. Photon transmission technique was used to monitor the optical transmittance and two-/four-probe methods were used for the electrical conductivity measurements. Two separate experimental sets were prepared. In the first set, the composite films were prepared at equal amounts of PS and rGO where the pH of the solution in which GO was reduced to rGO was changed from about 3 to 10. The second set includes the composite films which were prepared at different weight ratios of rGO which prepared at pH = 10. All of the composite films were annealed under the Infrared lamp and the annealing time was changed from 10 to 30 min to be able to understand the effect of the annealing time. It was observed that increasing annealing time starts the film formation at lower temperatures. Only the void closure stage of the film formation process could be observed for all composite films and increasing amount of rGO decreased the required energy for the void closure stage. POLYM. COMPOS., 2018. © 2018 Society of Plastics Engineers

INTRODUCTION

Graphene has gained attention of numerous researchers because of its unique properties [1–3] like excellent conductivity [1,4], a high surface area [5], a high aspect ratio [6] and high transmittance [7]. Because of these properties of graphene, it is used in many areas of applications in the industrial field such as; sensors, batteries, super capacitors, hydrogen storage and support for heterogeneous catalysts [8].

Correspondence to: O. Yargi; e-mail: oyargi@yildiz.edu.tr
Contract grant sponsor: Yildiz Tecnical University; contract grant number: 2016-01-01-KAP03.
DOI 10.1002/pc.25045
Published online in Wiley Online Library (wileyonlinelibrary.com).
© 2018 Society of Plastics Engineers

To date, several techniques have been established for the synthesis of graphene. However, mechanical cleaving (exfoliation), chemical exfoliation, chemical synthesis and thermal chemical vapor deposition, solvo-thermal synthesis, and the reduction of graphene oxide (GO) are the most commonly used methods today [9–13]. However, all synthesis methods have their own advantages as well as disadvantages depending on the final application of graphene. Chemical synthesis is the first method that demonstrated graphene synthesis by a chemical route. Chemical synthesis processes are performed at low temperature that makes it easier to fabricate graphene. It consists of the synthesis of graphite oxide, dispersion in a solution, followed by reduction with hydrazine. Functionalized graphene with different functional groups can be easily synthesized via this route.

Hummers' method is the most common method used for preparing GO [14] which uses strong oxidizing mixtures containing concentrated sulfuric acid (H_2SO_4) and oxidizing materials such as potassium permanganate ($KMnO_4$) and sodium nitrate ($NaNO_3$). In contrast to traditional Hummers' method, GO was prepared by increasing the amount of $KMnO_4$, and $NaNO_3$ which improves the efficiency of the oxidation process. This modified method provides a greater amount of hydrophilic oxidized graphene material. Moreover, GO produced by this method is more oxidized than that prepared by Hummers' method. When GO particles obtained from these two different methods were reduced in the same chamber with hydrazine hydrate (N_2H_4), it was observed that the yield of producing rGO in the modified method is higher.

The reduction methods have strong effects on the sample morphology and physical properties. Wettability, electrical conductivity, and transparency are strictly related to the chemical composition and the surface morphology of

the pristine GO sheets as well as to the conditions utilized for the specific fabrication processes [15].

Doping graphene into polymer can enhance the physical properties and leads to obtain composite materials for special purposes. GO group containing abundant oxygen, such as; epoxy, hydroxyl and carboxyl, can be well dispersed in a polymer matrix, due to its good interaction with polymer chains [8]. This is particularly interesting for the case of functional transparent coatings. Such coatings have potential applications in several fields, such as smart textiles, self-cleaning surfaces, biomaterials, microfluidics and microelectronics [16–19].

The optical properties of the latex films are affected by the annealing considerably. Three main stages occur during the annealing and at each stage the optical properties change depending on the changing internal structure of the latex film. These stages can be summarized as following: (1) Water evaporation and subsequent packing of polymer particles. (2) Deformation of the particles and getting close contact between the particles. This is observed for the particles with a glass transition temperature (T_g) which is less than or close to the annealing temperature (soft or low T_g latex). (iii) Particles with a T_g above the annealing temperature (hard or high T_g latex) stays undeformed at this stage. In the annealing of a hard latex system, deformation of particles first leads to void closure [20–22]. In some previous studies, small-angle neutron scattering method was used to study the latex film formation at molecular level by Sperling and co-workers [23] on compression-molded polystyrene (PS) film. Direct-nonradiative energy transfer (DET) method was employed to investigate the film formation process from dye-labeled polymeric particles [24–26]. Steady state fluorescence technique combined with DET was used to examine healing and interdiffusion processes in the dye labeled poly(methyl methacrylate) (PMMA) latex systems [27,28]. Photon transmission method has been performed to study latex film formation from PMMA and PS particles, using the UV–visible(UV–Vis) technique as a function temperature and time [29–31].

In this study, the effect of rGO on the optical transmittance and the electrical properties of PS latexes were carried out. The study was divided into two stages. In the first stage, the effect of the rGO particles prepared at different pH ranging from about 3 to 10 was examined. And, the effect of the weight ratio of the rGO particles prepared at a fixed pH, 10, was carried out at the second stage. The weight ratio of the rGO particles in the second stage was changed from about 3 to 18% (w/w).

Infrared (IR) lamp was used for annealing for all composite films and UV–Vis technique was used to monitor the optical transmittance. PS was used as a polymer matrix because it has a high resistivity, its properties are well-known; it is easy to process, it is soluble in a broad range of solvents, and its clarity allows dispersion of rGO to be optically observed at the micron scale [32,33]

EXPERIMENTAL

Materials

Synthesis of GO and Exfoliation to Few Layer GO. Graphite powder (0.5 g) (Alfa Aesar Graphite flake, natural, −325 mesh, 99.8% metal basis) and sodium nitrate (0.5 g) (Merck cryst. Extra pure) were placed in 23 mL concentrated H_2SO_4 aqueous solution (Merck, 95–98%). The ingredients were mixed in an ice-bath that had been cooled to 0°C. A 3 g of $KMnO_4$ (Merck, cryst. Extra pure) was added gradually with stirring and cooling, and the mixture was stirred at 35 ± 1°C for 60 min. A 40 mL of distilled water was added slowly and the temperature was increased to 90 ± 1°C. The mixture was stirred for 30 min at this temperature. Finally, 100 mL of distilled water and 3 mL 30% H_2O_2 aqueous solution were added after the reaction. The suspension was filtered while it was still warm. The resultant solid was dispersed in deionized water and centrifuged at 8,000 rpm for 15 minutes for two times and then dried at 40°C for 24 h in vacuum. The exfoliation of GO into few layer GO was achieved by ultrasonic homogenization. Briefly, 50 mg of as-synthesized graphitic oxide was redispersed in distilled water at 1 mg/mL concentration and allowed to ultrasonication for 45 min. The ultrasound irradiation was carried out on a SONIC VCX 750 model (20 kHz, 750 W) device which uses a direct immersion titanium horn operating at 40% amplitude.

A stock of few layer GO suspension with 1 mg/mL concentration was prepared by bath ultrasonicating in distilled water for 1 h. The pH value of the pure few layer GO solution was measured as 2.60 with pH meter (Thermo Fisher Scientific, Orion Star A211).

Hydrazine monohydrate (Sigma Aldrich, N_2H_4, 64–65%, reagent grade, 98%) with different mass ratios was added to few layer GO solution for adjusting their pH values. In the next step, the solutions were ultrasonicated for 5 min followed by microwave-assisted reduction.

Microwave-Assisted Reduction of GO to rGO. Few layer GO has been reduced to graphene during the microwave-assisted reactions carried out in a microwave accelerated reaction system (CEM, Mars 5). The Microwave irradiation was applied in a microwave oven with 1,600 W power at % 50 amplitude (2,450 MHz) for 5 min.

Polystrene. PS particles were produced via surfactant free emulsion polymerization process. The polymerization was performed batch-wisely using a thermostated reactor equipped with a condenser, thermocouple, mechanical stirring paddle, and nitrogen inlet. The agitation rate was 400 rpm and the polymerization temperature was controlled at 70°C. Water (100 mL) and styrene (5 g) were first mixed in the polymerization reactor where the temperature was kept constant (at 70°C). The potassium peroxodisulfate, which was used as an initiator (0.1 g), was dissolved in small amount of water (2 mL), and then was introduced to induce styrene polymerization. The polymerization was

 DOI 10.1002/pc

conducted during 18 h. The polymer has a high glass transition temperature (T_g = 105°C).

Film Preparation. Two sets were prepared from the dispersion of PS/rGO composites by placing the same number of drops on a glass plate with the surface area of 0.8 × 2.5 cm^2 and allowing the water to evaporate. In the first set, the latex films were prepared including rGO particles which were synthesized in the solution with changing pH (2.99, 3.23, 4.54, 6.32, and 10.00) and in the second set, the latex films were prepared including rGO particles with changing weight ratios from 3 to 18% (w/w). The rGO particles used in the second set were prepared at fixed pH = 10. Then the samples were separately annealed starting from 100°C below T_g of PS to 270°C for different times (10, 20, and 30 min) under IR lamb.

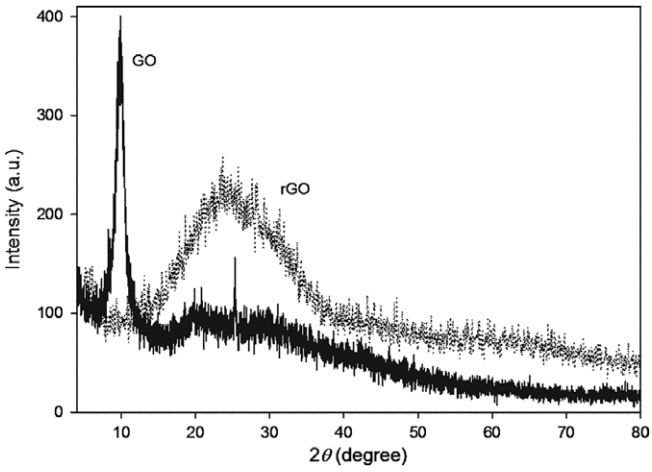


FIG. 1. XRD spectra of few layer GO (solid line) and rGO (dotted line) prepared at pH = 10.

MEASUREMENTS

X-ray diffraction

X-ray diffraction (XRD) patterns of the samples were obtained by using Philips Panalytical X'Pert-Pro diffractometer with a CuKα (λ = 0.1541874 nm) radiation. The scanning was performed at 40 kV and 40 mA. The crystallite size along the c-axis (L_c) was obtained from the (002) reflection of the XRD patterns using the Scherrer equation, which were recorded at a scan speed of 1°/min and a step size of 0.02° in the range of 5° ≤ 2θ ≤ 90°. The crystallite size along the axis (L_a) was calculated from the (100) Bragg peak. The (100) reflection is overlapped by the (101) reflection and had to be deconvoluted to obtain the position and the width of the peaks.

UV–Visible

Photon transmission measurements were performed by using UV–Vis spectrometer, B&W Tek. The transmittances of the films were detected at 800 nm. A glass plate was used as a substrate for all transmittance experiments and the measurements were carried out at room temperature.

Scanning Electron Microscopy

Scanning electron microscopy (SEM) analysis was used to investigate the surface morphology and the microstructure of PS and PS/rGO films. Non-conductive specimens were mounted on aluminum stubs using carbon tape and they are coated with gold by using a Polaron SC7610 Sputter in vacuum before the examination in the SEM. The surface morphology of the composite films was examined by Philips XL30 SFEG SEM at 5 kV and JEOL JIB-4501 MultiBeam Focused Ion Beam-SEM.

Electrical Conductivity

Electrical conductivity was performed by using a two and four probe method. For two-probe method, a direct current (DC) source meter and Keithley Model 6517a Electrometer which is an ultrahigh resistance meter at picoamper level was used and LucasLabs Pro4 probe was used for four-probe measurements. For the conductivity measurements, the samples were coated onto thin rectangular glass slabs with typical dimensions of 0.8 × 2.5 cm^2. The electrical contact was made using a silver paste. Electrical resistivities of the composite films were measured by alternating polarity technique for 15 s under 20 V alternating potential. The resistivity was converted to conductivity by taking the inverse of the resistivity.

RESULTS AND DISCUSSION

The XRD spectra given in Fig. 1 show (002) diffraction peak at 2θ = 9.76° for few layer GO and at 2θ = 25.16° for few layer reduced GO (rGO). The position can be easily influenced by the oxidation and the hydration level of GO sample [34,35]. The Bragg's equation [36] was used to calculate the distance between the graphene layers and found to be 9.1 Å for GO and 3.5 Å for rGO. It is reported that the pristine graphite exhibits a characteristic (002) peak at 2θ = 26.5° with the interlayer spacing of 3.4 Å. This increment in the interlayer spacing from 3.4 to 9.1 Å after the oxidation is assigned to the presence of the oxygen functional groups and water molecules on the surface of the GO layers. The reported interlayer distance of GO samples varies from 5.97 to 9.50 Å. The number of the layers was calculated as 4 and 1–2 for few layer GO and rGO, respectively. The Debye–Scherrer's equation [36] was used to calculate the size of the crystallites and found to be 3.58 and 0.45 nm for few layer GO and rGO, respectively. It was concluded based on these data that the reduction of GO to rGO was successfully carried out.

SEM images of the PS/rGO composite films annealed at 180°C for 10 min were given in Fig. 2. rGO particles used in these films were synthesized at different pH conditions and the pH values were denoted on the images.

The films with rGO synthesized at low pH values show more porous structure while the structure turns to be more

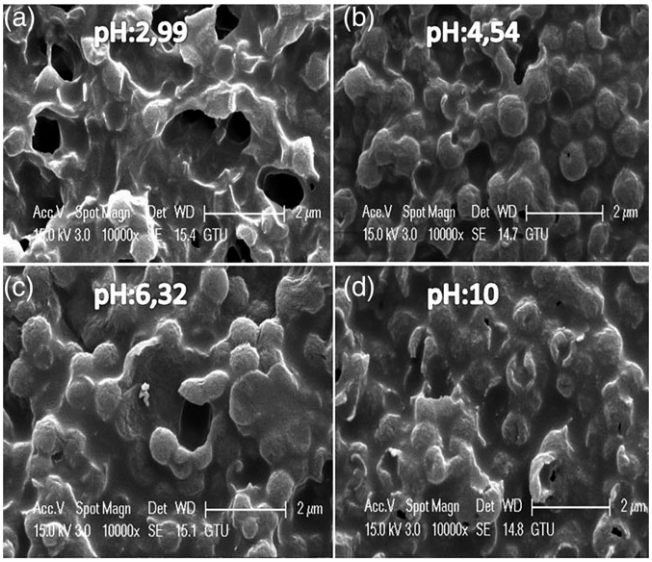


FIG. 2. SEM images of the PS/rGO (50/50, w/w) composite films annealed at 180°C. The pH values on the images show the pH values during the synthesis of rGO.

homogeneous when rGO particles prepared at higher pH were used. The reason for this is the structural change of rGO particles depending on the pH. When the reduction of the GO is performed at lower pH values, the resulting rGO particles become smaller and the planar structure is destroyed that is, they turn to be curved structures [15]. This random and the non-planar structures of rGO also affects the structure of the composite films and change the film structure to more heterogeneous and more porous as seen in Fig. 2a. When the pH of the solution used in the reduction of GO is increased, the rGO preserves its planar form and the structure of the composite film turns to be more homogeneous form as seen in Fig. 2d.

Optical transmittance variations of the composite films depending on the annealing temperature were represented in Fig. 3. The numbers in the legends indicate the pH values of the solution in which GO was reduced to rGO. The transmittance is very low for the films with rGO prepared at low pH values as expected. As mentioned before, the structure of rGO prepared at low pH is random, non-planar and tend to

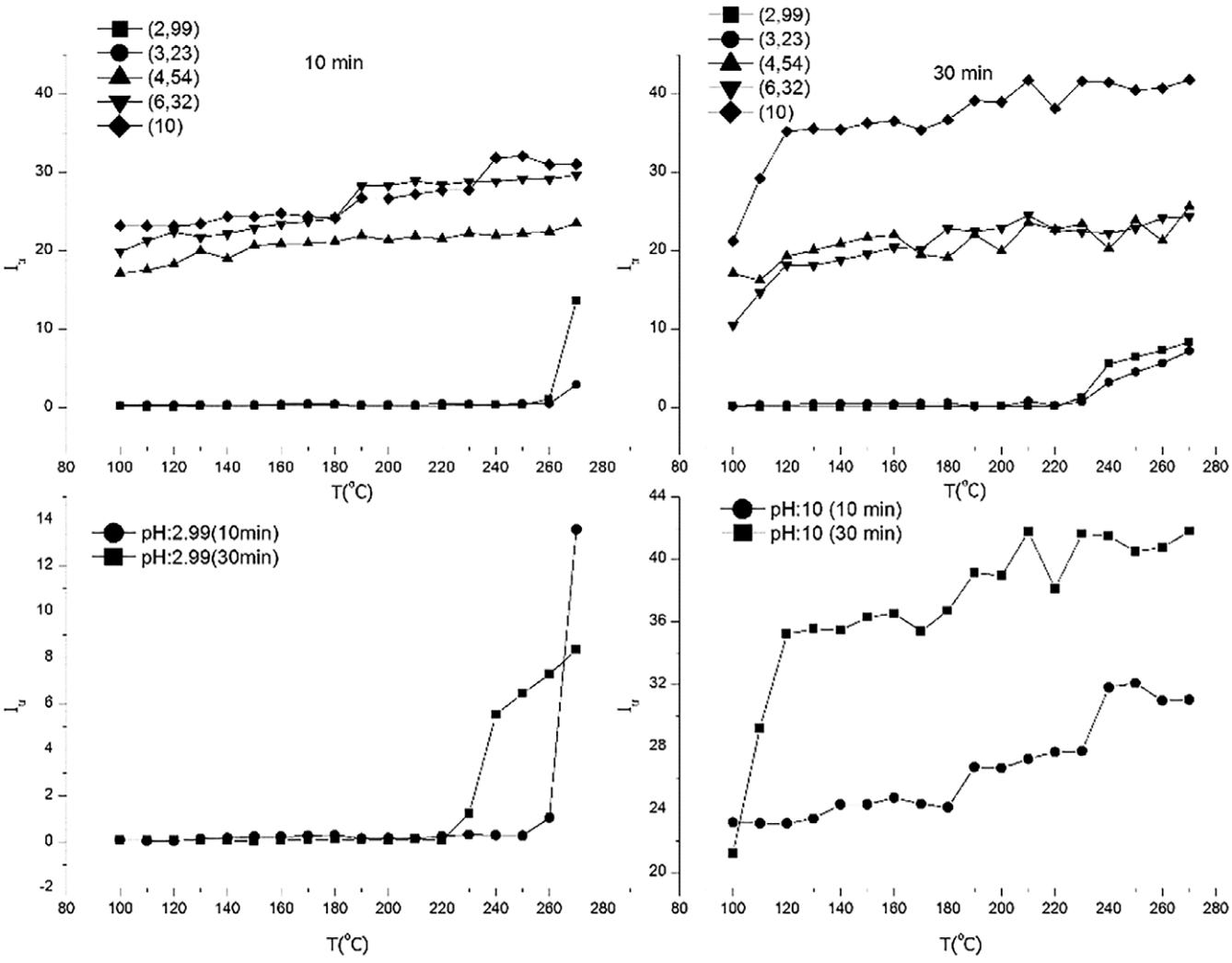


FIG. 3. Transmittance variation of the composite films depending on the annealing temperatures and the pH of the solution used for the reduction of GO.

 DOI 10.1002/pc

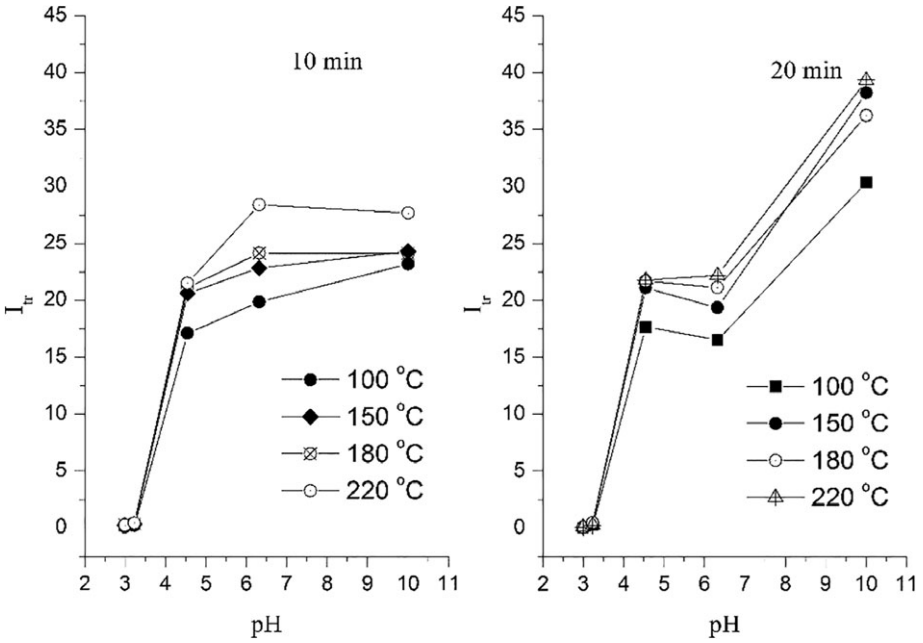


FIG. 4. Optical transmittance of the composite films versus pH of the solution in which GO was reduced to rGO.

agglomerate which results in an increasing scattering of the light passing through it. When the pH is increased the planar and ordered structures is recovered and change the structure of the film to more homogeneous form which results in increasing optical transmittance. For the films with rGO prepared at lower pH, almost no effect of the annealing time was observed below 220°C. On the other hand, a considerable effect of the annealing time was observed for the films with rGO prepared at pH = 10. At low pH values, probably, the PS particles flow through the holes inside and between these non-planar and agglomerated rGO particles and this flow does not change the structure of the whole film considerably. Thus, only a slight increase in the optical transmittance was observed depending on the annealing temperature. At high pH (pH = 10), both the transmittance and the rate of the increase in the transmittance are bigger than the films including rGO prepared at low pH for both annealing times. In addition, a sharp increase was observed at 110°C for 30 min annealing time which indicates the starting of the film formation process. At this pH, the PS particles flow through the voids between the particles and turn the structure of the film to the more homogeneous form. For shorter annealing times, this sharp increase in the transmittance was not observed and this shows that the matrix is highly resistive for the motion of the PS particles and it takes much more time for the homogeneous distribution of PS particles inside the film. Also, increasing the annealing time lowers the required temperature for starting the film formation process for the films including rGO prepared at lower pH values as seen in Fig. 3c.

In Fig. 4, the optical transmittance variation of the composite films depending on the pH of the solution in which rGO was prepared. Four annealing temperatures with two different annealing times were given as example in this figure. It is clearly seen from this figure that the pH of the solution has a considerable effect on the optical transmittance of the composite films. When the pH of the solution increases, agglomeration of rGO disappears and planar and more ordered structure can be obtained which makes the film more homogeneous and increase the optical transmittance. For smaller annealing times, the optical transmittance first increases and then goes to saturation while it is continuously increases for the films annealed for longer times. This is because of the mobility of the particles in the matrix. As mentioned earlier, the matrix acts as a resistive medium against the motion of the particles inside the matrix and it takes more time to distribute the particles through the film.

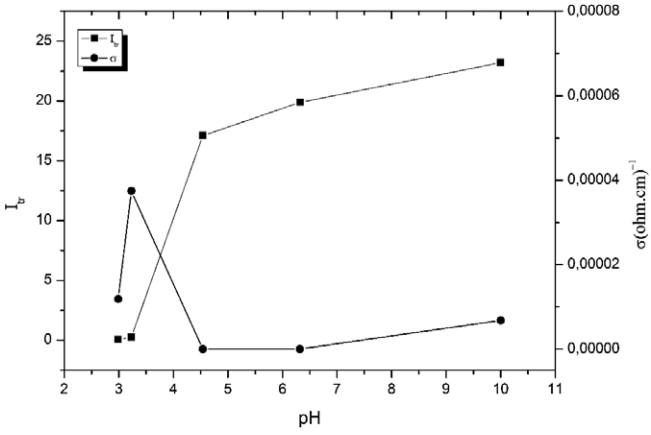


FIG. 5. Comparison of the optical transmittance and the conductivity of the composite films depending on the pH of the solution in which GO was reduced to rGO. The composite films were annealed at 100°C and the amount of rGO in the composite film 50% (w/w). 2-probe technique was used for the electrical conductivity measurements.

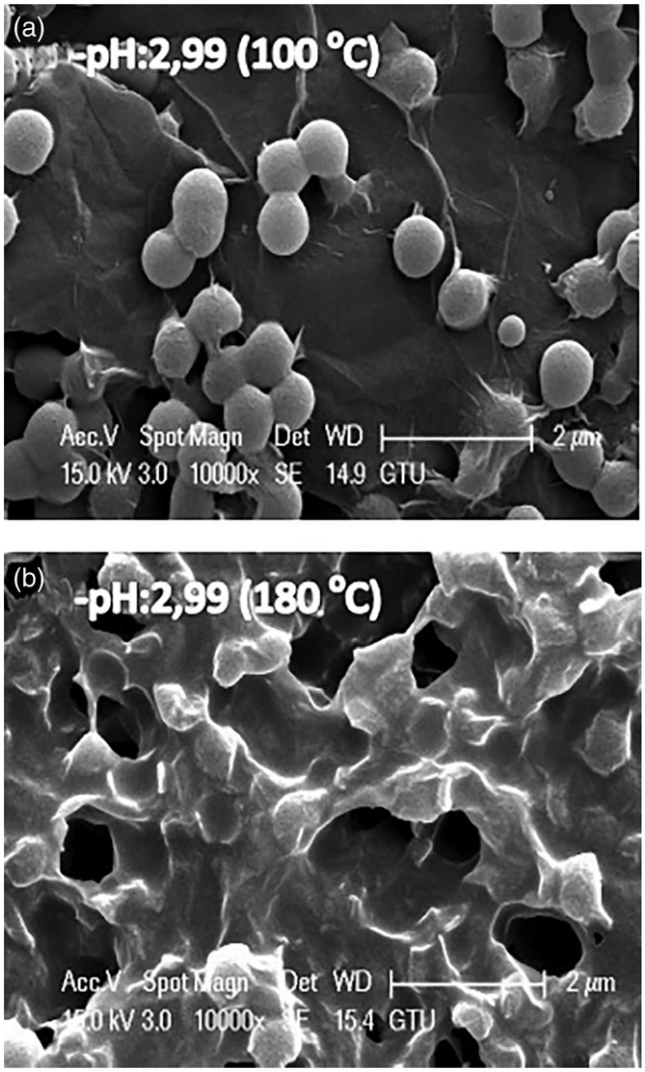


FIG. 6. The SEM images of the composite films annealed at 100 and 180°C. The weight fraction, w/w, of PS and rGO is 50/50.

Conductivity and optical transmittance behave inversely with respect to the pH of the solution in which GO was reduced to rGO as seen in Fig. 5 where the conductivity increases while the optical transmittance decreases. The composite films used in this experiment were annealed at 100 °C and to be able to explain this behavior, first the SEM images given in Fig. 6 must be taken into account. As seen in Fig. 6, at T = 100°C, which is lower than T_g of PS (105°C), the PS particles almost preserve their structures and just started to coalescence to rGO particles. However, at T = 180°C, the PS particles melted away through the surface and through the voids in the matrix. The PS particles seen at 100°C act as elastic and insulating barriers between the rGO particles. At high pH values, the rGO particles are nearly planar and thus the PS particles prevent to physically touch enough number of rGO particles to percolate. This results in a considerable decrease in the conductivity of the composite films. At low pH values the rGO particles are not planar and agglomerate to construct bigger and percolated rGO clusters which results in a comparably higher conductivity. But these agglomerated rGO clusters behave like a scattering centers for the light and decrease the optical transmittance of the composite film.

In Figs. 7 and 8a, the variations of the optical transmittance of the composite films with respect to annealing temperature and maximum transmittance at 220°C were represented, respectively. The amount of rGO, which was prepared in a solution with pH of 10, was changed from 0 to 18% (w/w) for these composite films. The first thing we see from these figures that the overall optical transmittance decreases as the amount of rGO increases. This clearly shows that rGO particles behave as scattering centers in the composite film. Another important point is that the film formation can be realized for all rGO amounts except 18% rGO [37]. For the composite film with 18% rGO, only the void closure step was observed. The rGO particles probably block the PS particles to move through the polymer boundaries and thus it will not be possible to observe both steps for the composite films which include rGO more than 18%. This result may indicate that there is a critical rGO concentration above which the film formation cannot be observed completely. This is also in accordance with the results given in Fig. 3 where the film formation process was clearly monitored only at highest pH and at longer annealing times.

The activation energies for the void closure are calculated by fitting the experimental data to the following equation [37].

$$I_{tr}(T) = S(t)\exp\left(-\frac{3\Delta H}{k_B T}\right) \quad (1)$$

where $S(t) = (yt/2AC)^3$, k_B is the Boltzmann's constant, ΔH is the activation energy of the void closure stage, and I_{tr} is the transmittance at 800 nm. The parameters y, t, and C in $S(t)$ are the surface energy, time, and integration constant, respectively. The parameter A is defined as $A = (N_A h/V)e^{-\Delta S/k_B}$ where N_A is Avogadro's number, h is Planck's constant, V is the molar volume, and ΔS is the entropy change.

In Fig. 8b, $(I_{tr})^{max}$ decreases with increasing rGO content and shows a sudden decrease at 7% (w/w) rGO in composite film. This predicts a percolation threshold (R_c) behavior of rGO in polymer matrix.

In Fig. 9, the calculated void closure activation energies depending on the amount of rGO were given. Here, we assumed that two different void closure processes took place during the annealing and healing process could not be observed. This result was reached by the values of the activation energies calculated from the optical transmittance temperature curves that is, the activation energies of the healing process were found to be smaller than those of

 DOI 10.1002/pc

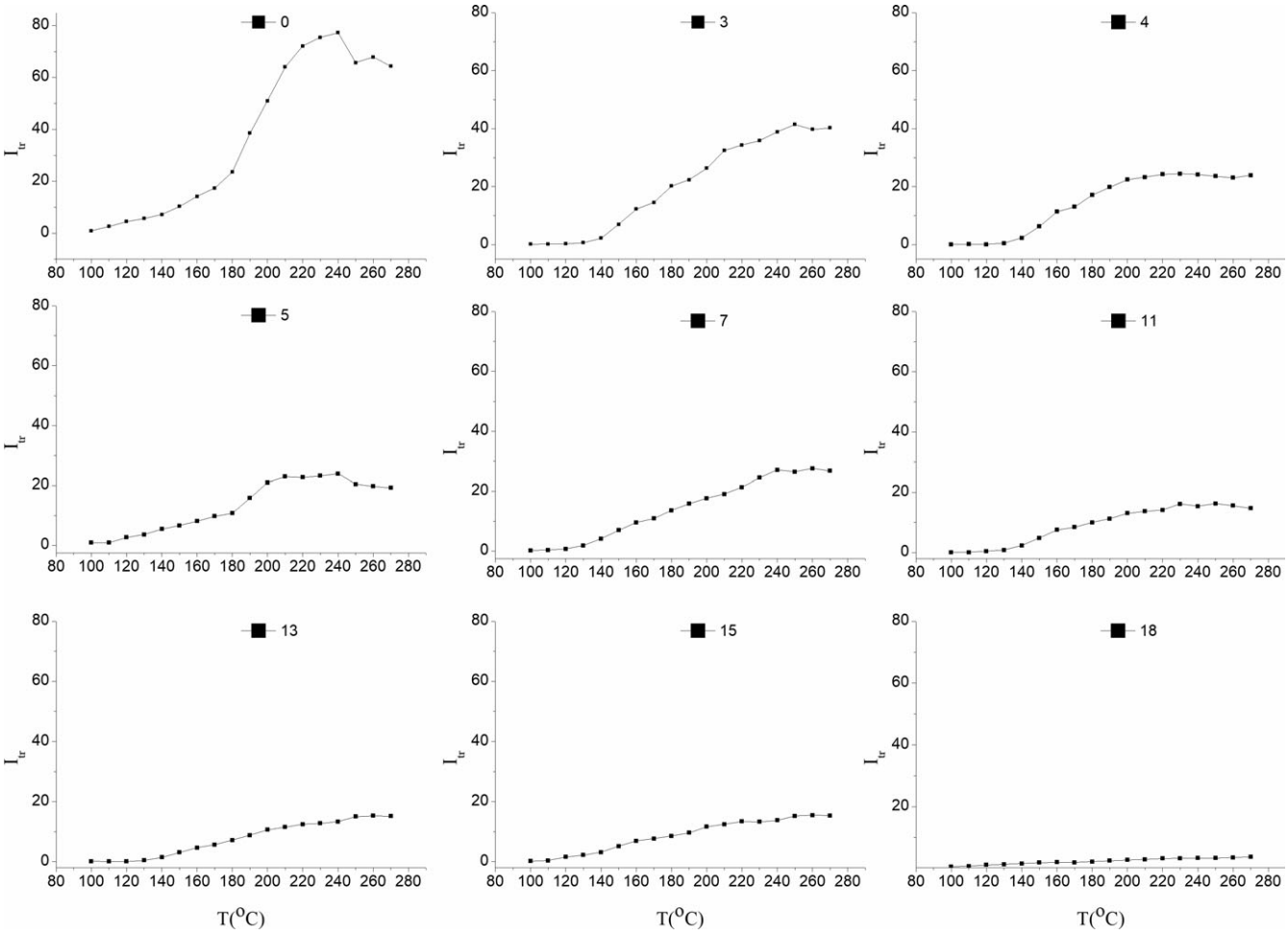


FIG. 7. The variation of the optical transmittance with respect to annealing temperature for the composite films including different amount of rGO.

void closure process. But, this was not physically meaningful because moving particles through the voids requires less energy than to move polymers through the boundaries [38]. Therefore, we assumed that only two different void closure processes could be present in this system. In the first void closure stage probably the bigger voids between the rGO particles are filled by the PS polymer particles and then the smaller voids between the PS particles are filled in the second stage. The required energy is smaller for the second stage (down triangles) as expected. In addition, the void closure activation energies in the first stage decrease as the amount of rGO is increased. The rate of the decrease in the second stage is very small and can be neglected when compared with the first stage. This result also supports the above explanation because as the amount of rGO increases the number of the bigger voids increases and the required energy to move the PS particles through these bigger voids decreases. However, in the second stage, since the PS particles and the voids between these particles are almost identical in size, the required energy to fill these voids between the PS particles is almost constant and it is not affected by the amount of rGO.

The activation energies at the void closure stage of the film formation process with respect to the pH of the solution in which GO was reduced to rGO were given in Fig. 10. The results are in accordance with the results given in Fig. 8 where two-stage void closure was observed. The activation energies at the first stage decreases as the pH increases. This is an expected result because when the pH of the solution increases bigger sized and planar type rGO structures are obtained as mentioned before and thus the size of the voids between these bigger sized and planar rGO structures gets bigger. The required energy to move the PS particles through these voids between the rGO particles decreases as the size of the rGO particles gets bigger with the increasing pH. At the second stage of the void closure again no considerable change depending on the pH was observed which is in accordance with the observations in Fig. 9.

Electrical conductivity measurements of the composite films with varying amount of rGO, from 2.5 to 18% (w/w), was also evaluated as seen in Fig. 11. It is clearly seen that the overall conductivity of the composite films is small and depending on the amount of rGO it passes through a peak.

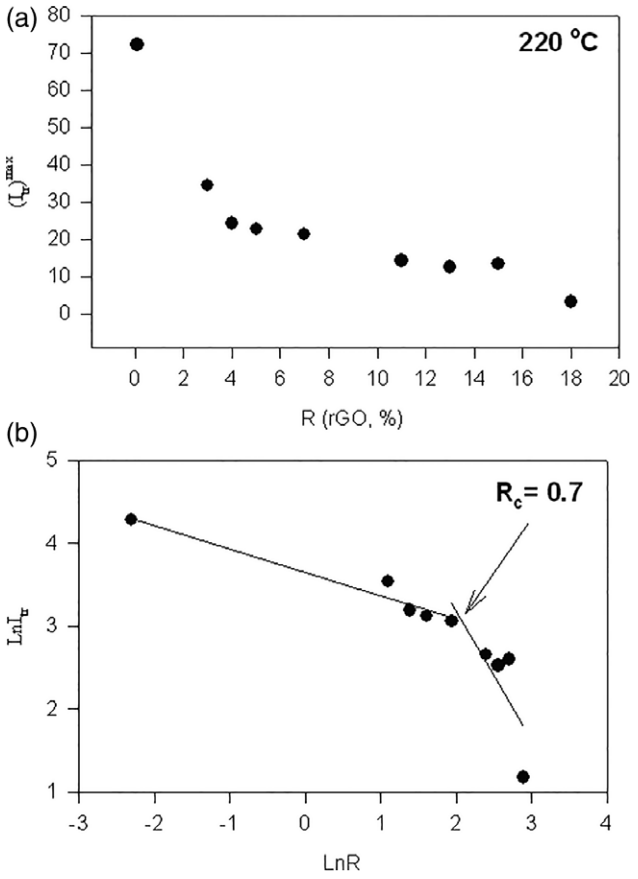


FIG. 8. (a) Maximum transmitted light intensity change versus PS/rGO composite films at 220°C. (b) Critical value of rGO amount in the composite films.

The first observation shows that rGO did not affect the electrical conductivity of PS latex films considerably. This may be due to the physical structure and the aggregation behavior of rGO particles. These properties probably prevent the formation of open channels through the film to move the charge carriers efficiently. The second

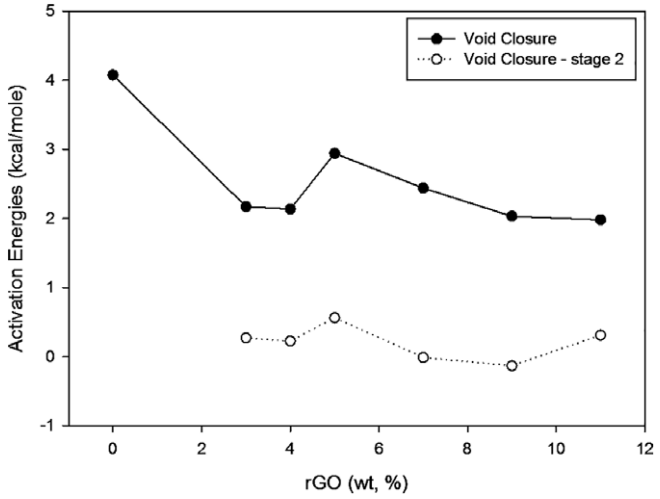


FIG. 9. Activation energies versus amount of rGO in the composite films.

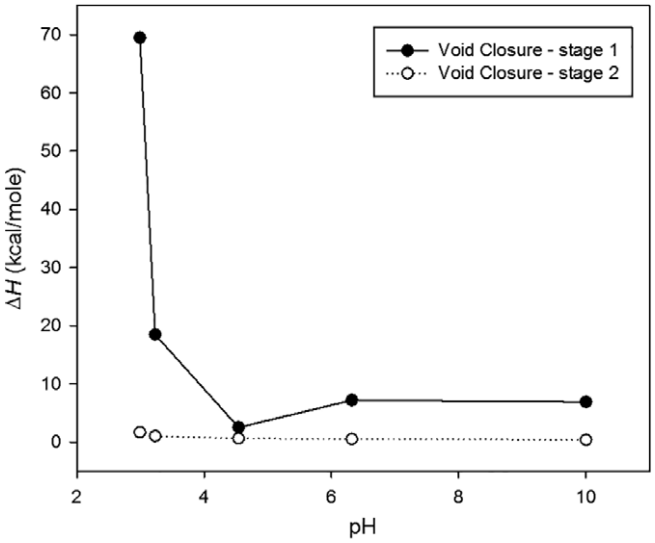


FIG. 10. Activation energies at the void closure stage with respect to pH of the solution in which rGO was prepared.

observation in this figure, the peak in the electrical conductivity, may be explained in terms of the percolation of rGO particles. At a specific amount of rGO, probably some percolated clusters are present to conduct electrical current. These two points can be deduced from the SEM images given in Fig. 12 where the SEM images of the composite films including 7, 9, 13, and 18% (w/w) rGO were represented, respectively. Here, it is clearly seen that the distribution of rGO through the film is bigger for the composite film with 9% rGO than the others. This behavior affects the electrical conductivity considerably and as seen in Fig. 11 the conductivity increases for this amount of rGO. At the other rGO contents, 7, 13, and 18%, rGO particles mostly aggregated and constructed smaller rGO rich regions. These findings are also consistent with Fig. 8b where the starting point of percolation is 7%. Since these small

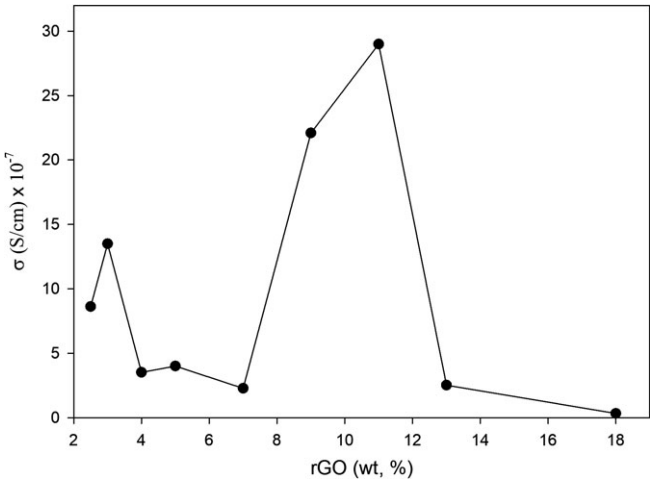


FIG. 11. Conductivity of the composite films depending on the amount of the rGO in the composite films annealed at 100°C. The pH of the solution in which GO was reduced to rGO is 10.00 and 4-probe technique was used for the electrical conductivity measurements.

DOI 10.1002/pc

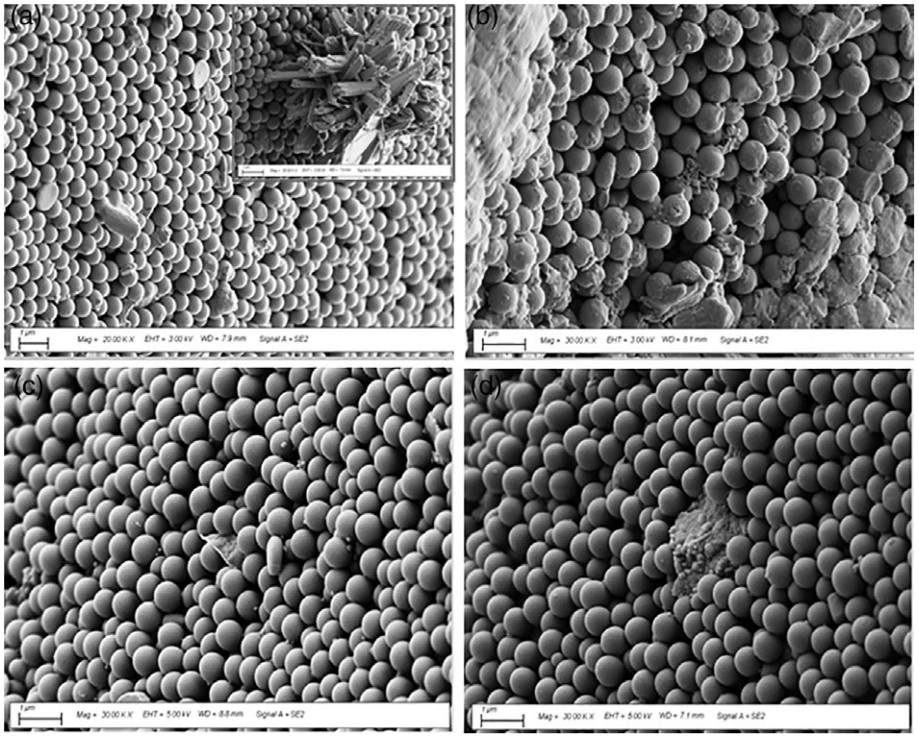


FIG. 12. SEM images of the composite films including 7, 9, 13, and 18% (w/w) rGO.

regions do not percolate, their contribution to the electrical conductivity is very small.

CONCLUSIONS

Depending on the results obtained from the experiments, it was concluded that rGO strictly affects the structure of the composite films. When rGO particles prepared at low pH values are used, the structure of the composite film becomes heterogeneous but when rGO particles prepared at higher pH values are used the structure turns to be comparably more homogeneous. Therefore, if a composite film with high optical transmittance is intended, rGO prepared at high pH values must be used.

The concentration of rGO used in the composite film is very important for obtaining a composite film with desired structure. In this study, it was concluded that, a complete film formation could not be observed for the films including rGO above 18% weight ratio.

Electrical conductivity of the composite films is very low and it decreases much more when rGO particles prepared at higher pH values are used. At specific rGO content, the rGO particles starts to percolate through the film and so the electrical conductivity reaches the maximum value.

ACKNOWLEDGMENT

We want to thank Yildiz Tecnical University, Coordination of Scientific Research Projects for financial supporting of our project numbered 2016-01-01-KAP03.

REFERENCES

1. K.S. Novoselov, A.K. Geim, S.V. Morozov, D. Jiang, Y. Zhang, S.V. Dubonos, I.V. Grigorieva, and A.A. Firsov, *Science*, **306**, 666 (2004).
2. T. Kuila, S. Bose, A.K. Mishra, P. Khanra, N.H. Kim, and J. H. Lee, *Prog. Mater.Sci.*, **57**, 1061 (2012).
3. H. Kim, A.A. Abdala, and C.W. Macasko, *Macromolecules*, **43**, 6515 (2010).
4. K.I. Bolotin, K.J. Sikes, Z. Jiang, M. Klima, G. Fudenberg, J. Hone, P. Kim, and H.L. Stormer, *Solid State Commun.*, **146**, 351 (2008).
5. M.D. Stoller, S.J. Park, Y.W. Zhu, J.H. An, and R.S. Ruoff, *Nano Lett.*, **8**, 3498 (2008).
6. O.C. Compton, S. Kim, C. Pierre, J.M. Torkelson, and S. T. Nguyen, *Adv. Mater.*, **22**, 4759 (2010).
7. R.R. Nair, P. Blake, A.N. Grigorenko, K.S. Novoseleov, T. J. Booth, T. Stauber, N.M.R. Peres, and A.K. Geim, *Science*, **320**, 1308 (2008).
8. R.J. Rodbari, R. Wendelbo, L.C.L.A. Jamshidi, E. P. Hernandez, and L. Nascimento, *J. Chil. Chem. Soc.*, **61**, 3 (2016).
9. W.-S. Jiang, Z.-B. Liu, W. Xin, X.-D. Chen, and J.-G. Tian, *Nanotechnology*, **27**, 095301 (2016).
10. C. Berger, *Science*, **312**, 1191 (2006).
11. M. Choucair, P. Thordarson, and J.A. Stride, *Nat. Nanotechnol.*, **4**, 30 (2009).
12. S. Stankovich, D.A. Dikin, R.D. Piner, K.A. Kohlhaas, A. Kleinhammes, Y. Jia, Y. Wu, S.T. Nguyen, and R. S. Ruoff, *Carbon*, **45**, 1558 (2007).
13. W. Chen, L. Yan, and P.R. Bangal, *Carbon*, **48**, 1146 (2010).

14. W.S. Hummers and R.E. Offeman, *J. Am. Chem. Soc.*, **80**, 1339 (1958).
15. A. Furio, G. Landi, C. Altavilla, D. Sofia, S. Iannace, A. Sorrentino, and H.C. Neitzert, *Nanotechnology*, **28**, 054003 (2017).
16. P. Roach, N.J. Shirtcliffe, and M.I. Newton, *Soft Matter*, **4**, 224 (2008).
17. P.N. Manoudis, I. Karapanagiotis, A. Tsakalof, I. Zuburtikudis, and C. Panayiotou, *Langmuir*, **24**, 11225 (2008).
18. W. Hou and Q. Wang, *J. Colloid Interface Sci.*, **316**, 206 (2007).
19. Z. Wu, H. Han, W. Han, B. Kim, K.H. Ahn, and K. Lee, *Langmuir*, **23**, 7799 (2007).
20. P.R. Sperry, B.S. Snyder, M.L. O'Dowd, and P.M. Lesko, *Langmuir*, **10**, 2619 (1994).
21. J.K. Mackenzie and R. Shuttleworth, *Proc. Phys. Soc.*, **62B**, 833 (1949).
22. J.L. Keddie, *Mater. Sci. Eng.*, **R21**, 101 (1997).
23. K.D. Kirn, L.H. Sperling, and A. Klein, *Macromolecules*, **26**, 4624 (1993).
24. O. Pekcan, M.A. Winnik, and M.D. Croucher, *Macromolecules*, **23**, 2673 (1990).
25. Y. Wang, C.L. Zhao, and M.A. Winnik, *J. Chem. Phys.*, **95**, 2143 (1991).
26. Y. Wang and M.A. Winnik, *Macromolecules*, **26**, 1347 (1993).
27. M. Canpolat and O. Pekcan, *J. Polym. Sci. Polym. Phys. Ed.*, **34**, 691 (1996).
28. O. Pekcan and E. Arda, Encyclopedia of Surface and Colloid Science, Marcel and Dekker, 2691 (2002).
29. O. Pekcan, E. Arda, V. Bulmus, and E. Piskin, *J. Appl. Polym. Sci.*, **77**, 866 (2000).
30. E. Arda, F. Ozer, E. Piskin, and O. Pekcan, *J. Coll. Interface Sci.*, **233**, 271 (2001).
31. E. Arda and O. Pekcan, *Polymer*, **42**, 7419 (2001).
32. J. Lowell and A.C. Rose-Innes, *Adv. Phys.*, **29**, 947 (1980).
33. C.B. Duke and T.J. Fabish, *Phys. Rev. Lett.*, **37**(16), 1075 (1976).
34. D. Akyüz, B. Keskin, U. Sahintürk, and A. Koca, *Appl. Catal. B: Environ.*, **188**, 217 (2016).
35. H. Berber, E. Ucar, and U. Sahinturk, *Colloids and Surfaces A: Physicochemical and Engineering Aspects*, **531**, 56 (2017).
36. B.E. Warren, *X-Ray Diffraction*, Dover Publications, New York (1969).
37. O. Pekcan and F. Kemeroglu, *J. Appl. Polym. Sci.*, **72**, 981 (1999).
38. O. Yargi, A. Gelir, M. Ozdogan, C. Nuhoglu, and A. Elaissari, *J. Appl. Polym. Sci.*, **133**, 15 (2016).

 DOI 10.1002/pc